A&A 543, A32 (2012)
DOI: 10.1051/0004-6361/201118192

Astronomy & Astrophysics

Rotation-stimulated structures in the CN and C_3 comae of comet 103P/Hartley 2 close to the EPOXI encounter⋆,⋆⋆

W. Waniak[1], G. Borisov[2], M. Drahus[3], and T. Bonev[4]

[1] Astronomical Observatory of the Jagiellonian University, Orla 171, 30-244 Krakow, Poland
e-mail: waclaw.waniak@uj.edu.pl
[2] Institute of Astronomy of the Bulgarian Academy of Sciences, 72 Tsarigradsko Chaussee Blvd., 1784 Sofia, Bulgaria
e-mail: gborisov@astro.bas.bg
[3] University of California at Los Angeles, 595 Charles E. Young Dr. East, Los Angeles, CA 90024, USA
e-mail: mdrahus@ucla.edu
[4] Institute of Astronomy of the Bulgarian Academy of Sciences, 72 Tsarigradsko Chaussee Blvd., 1784 Sofia, Bulgaria
e-mail: tbonev@astro.bas.bg

Received 30 September 2011 / Accepted 1 April 2012

ABSTRACT

Context. In late 2010, a Jupiter family comet 103P/Hartley 2 was the subject of an intensive world-wide investigation. On UT October 20.7, the comet approached the Earth within only 0.12 AU, and on UT November 4.6 it was visited by the NASA EPOXI spacecraft.
Aims. We joined this international effort and organized a ground-based observing campaign with three key goals to: (1) measure the parameters of the nucleus rotation in a time series of CN; (2) investigate the compositional structure of the coma by comparing the CN images with nightly snapshots of C_3; and (3) investigate the photochemical relation of CN to HCN, using the HCN data collected nearly simultaneously with our images.
Methods. The images were obtained through narrowband filters using the two-meter telescope of the Rozhen National Astronomical Observatory. They were taken over four nights about the moment of the EPOXI encounter. Image processing methods and periodicity analysis techniques were used to identify transient coma structures and investigate their repeatability and kinematics.
Results. We observe shells, arc-, jet- and spiral-like patterns that are very similar for the CN and C_3 comae. The CN features expanded outwards with the sky-plane projected velocities of between 0.1 to 0.3 km s^{-1}. A corkscrew structure, observed on November 6, evolved with a much higher velocity of 0.66 km s^{-1}. The photometry of the inner coma of CN shows variability with a period of 18.32 ± 0.30 h (valid for the middle moment of our run, UT 2010 Nov 5.0835), which we attribute to the nucleus rotation. This result is fully consistent with independent determinations around the same time by other teams. The pattern of repeatability is, however, imperfect, which is understandable given the suggested excitation of the rotation state, and the variability detected in CN correlates well with the cyclic changes in HCN, but only in the active phases. The identified coma structures, along with the snapshot of the nucleus orientation obtained by EPOXI, enable us to estimate the spin axis orientation. We obtain RA = 122°, Dec = +16° (epoch J2000.0), neglecting at this point the rotational excitation.

Key words. comets: individual: 103P/Hartley 2 – techniques: photometric – techniques: imaging spectroscopy

1. Introduction

103P/Hartley 2 (hereafter 103P) is a Jupiter family comet, which currently has a perihelion at 1.06 AU and orbits the Sun with a 6.47-year period. Owing to its frequent perihelion passages, the comet was relatively well-characterised prior to its 2010 apparition (see e.g. Arpigny et al. 1993; Weaver et al. 1994; Crovisier et al. 1999; Colangeli et al. 1999; Epifani et al. 2001), although no information about the nucleus rotation was obtained.

The state of its rotation is, however, of great interest because it is one of the parameters that can help us to establish the lifetime of a cometary nucleus. It was realised long ago that a nucleus rotating faster than a certain limit (see e.g. Davidsson 2001) must be disrupted by a centrifugal force. On the other hand, knowledge of this parameter enables a proper interpretation of the observational data and their conversion to the physical quantities (such as the total production rates and relative abundances) which can be compared among comets.

The rotation period of 103P was first measured at 16.4 ± 0.2 h (Meech et al. 2011) shortly after the comet was selected as the target of the NASA EPOXI mission. The studies of the rotation continued as the comet became active. The EPOXI-based imaging and photometry (A'Hearn et al. 2011), as well as ground-based observations (see Meech et al. 2011 for an overview of the ground-based results), show that the rotation period was increasing with time and that the nucleus was most probably rotating in an excited mode.

Although indications of possible changes in the spin rate among comets have been reported before for some objects (e.g. C/1990 K1 (Levy), C/2001 K5 (LINEAR), 2P/Encke, 6P/d'Arrest, 10P/Tempel 1), the first unequivocal measurement of a slow decrease in the rotation period was obtained only recently for comet 9P/Tempel 1 (Belton & Drahus 2007; Belton et al. 2011). Model computations (e.g. Gutiérrez et al. 2003) show that emission of matter from active vents occupying a small fraction of an irregularly-shaped rotating nucleus

⋆ Based on data collected with two-meter RCC telescope at Rozhen National Astronomical Observatory.
⋆⋆ Appendix A and movies are available in electronic form at http://www.aanda.org

can produce a significant net torque. Owing to this effect, cometary rotation can evolve from the principal-axis toward the non-principal-axis (excited) mode after a couple of perihelion passages and remain in this state during the next tens of orbital revolutions. The problem of rotational excitation is important for the long-term evolution of cometary nuclei as the relaxation timescale has not yet been well-established (e.g. Samarasinha et al. 2004). Despite the suggestion of some authors (e.g. Belton 1991; Jewitt 1992) that most short-period comets should be in excited spin states, only three such cases have been reported: 2P/Encke (Belton et al. 2005), 29P/Schwassmann-Wachmann 1 (Meech et al. 1993), and 1P/Halley (Belton et al. 1991). The recent observational results for 103P show that its nucleus – having been observed in an excited and decelerated rotation state – is the first known comet in which the two processes have been found to occur at the same time. Moreover, thanks to the EPOXI mission, which enbled detailed measurements of the nucleus characteristics, this exceptional object is a unique laboratory to test our theories about the rotational dynamics of cometary nuclei.

Impressive images of 103P's nucleus obtained by EPOXI (A'Hearn et al. 2011) show an elongated body with tips of different sizes, the smaller one being insolated and active at the encounter. The nucleus is found to precess about the longest axis of inertia with the period of 18.34 ± 0.04 h and roll about the shortest axis of inertia (longest nucleus extent) with the probable period of 27.79 ± 0.31 h (both at the epoch of the EPOXI encounter). The two periodicities are nearly commensurate in 2:3 resonance, which causes the activity pattern to repeat every three precession cycles – a property also observed in ground-based HCN data (Drahus et al. 2011).

In this work, we analyse transient features in the CN and C_3 comae. In particular, the time series of CN is used to examine the kinematics, repeatability, and periodicity in the framework of the nucleus precession-roll scenario. We also determine the spin axis orientation of the nucleus. Our campaign was realized simultaneously with the HCN monitoring at IRAM 30-m (Drahus et al. 2011, 2012), which makes it possible to investigate the connection between HCN and CN. Although the HCN molecule is assumed to be the main donor of cometary CN (e.g. Bockelée-Morvan & Croviser 1985), this idea remains somewhat controversial (e.g. Fray et al. 2005).

2. Observations and data reduction

Observations of 103P were carried out on the four photometric nights of November 2, 4, 5, and 6, 2010, including the date (though not the moment) of the EPOXI encounter. The last night before the encounter, i.e. November 3, 2010, was also allocated but lost owing to bad weather. We observed with the two-channel FoReRo2 focal reducer (Jockers et al. 2000) mounted at the Cassegrain focus of the two-meter Ritchey-Chrétien-Coudé telescope of the Rozhen National Astronomical Observatory (Bulgarian Academy of Sciences). In the blue channel, we used a Photometrics CE200A-SITe CCD, and in the red channel a VersArray 512B CCD. Both CCDs have square-shaped 24-μm pixels, and give an image scale of 0.89 arcsec pix^{-1}, i.e. ~100 km at the comet nucleus.

In this work, we present the results of imaging in the blue channel and our remaining data will be presented in a subsequent paper. Emission bands of CN and C_3 were observed through the HB filters (Farnham et al. 2000) at 387 nm and 406 nm respectively; dust was observed through an interference filter at 443 nm. All exposures were 600 s with non-sidereal tracking on the comet. We obtained a couple of hours long series of CN images and snapshots of C_3 and dust. Reduction of the images included, in addition to the standard steps, removal of cosmic ray hits (CRH) and stellar profiles. We stacked consecutive images in pairs and cleaned them using the procedure described in Appendix A. In this way, we obtained 31 clean stacks for CN, 7 for C_3, and 7 for dust. The mid-exposure moments for the co-added images were corrected for the travel time of light. The statistics of the observations and the geometric circumstances, are presented in Table 1.

Table 1. Statistics of the images and geometric properties.

UT Date Nov. 2010	r^a [AU]	Δ^b [AU]	ϕ^c [°]	Number of exposures^d CN	C_3	dust
2.96–3.10	1.062	0.150	58.7	11/6	2/1	4/2
4.94–5.16	1.064	0.158	58.8	20/10	4/2	2/1
5.93–6.16	1.066	0.163	58.8	17/9	3/2	3/2
6.96–7.17	1.067	0.167	58.7	11/6	3/2	3/2

Notes. [a] Heliocentric distance. [b] Topocentric distance. [c] Topocentric phase angle (i.e. Sun-comet-observer angle). [d] Numbers of original/stacked images.

To enhance the visibility of faint coma structures, we proceeded in a similar way as for comet 8P/Tuttle (Waniak et al. 2009). This approach assumes and critically depends on the constant heliocentric distance of the comet and constant observing geometry in the analysed set of images – conditions that are well-satisfied for our short run (see Table 1). In such a case, the only reason for coma variability can be transient phenomena produced by e.g. unstable and/or periodically changing mass ejection. First, we converted the scales of the individual stacked images to the same topocentric distance for UT 2010 Nov. 5.0. Then a series of the rescaled frames for a given filter was used as an input to our novel technique: the *iterative image decomposition*, which extracts the time-invariant coma profile, and produces a series of images for the residual, time-dependent component. Our iteration loop contains two steps: (i) rescaling image signal by a factor followed by (ii) stacking such modified images into a mean frame. The normalization factors are adjusted with respect to this mean frame taken as a reference. The procedure begins with stacking of the original input frames with no normalization (i.e. the factors are set equal to unity). In the subsequent iterations, we stacked not the whole images but only the parts that do not change their profiles from frame to frame. These stable parts made it possible to compute the factors for signal rescaling. To detect and avoid pixels containing signatures of temporary signal enhancement, we applied the $K\sigma$ criterion for the pixel value difference between the individual normalised frame and the mean image. After a number of iterations when the mean profile appeared stable, we took this profile as the time-invariant coma pattern and subtracted it from the individual, normalised input frames, obtaining a series of *residual images*. Our experience shows that these images are photometrically related to each other to a much higher precision than can be achieved when performing the calibration using standard stars and nightly extinction coefficients. This approach also has other advantages over typical image enhancement procedures. It generally preserves photometric information, so the transient structures can be analysed quantitatively. Moreover, the level of enhancement does not depend on either position, shape, or size of a feature, if only the area of this feature is significantly smaller than the total area of the analysed part of the coma, and if the series of input images sufficiently samples the time variability of the coma profile. As we did not subtract the light scattered by

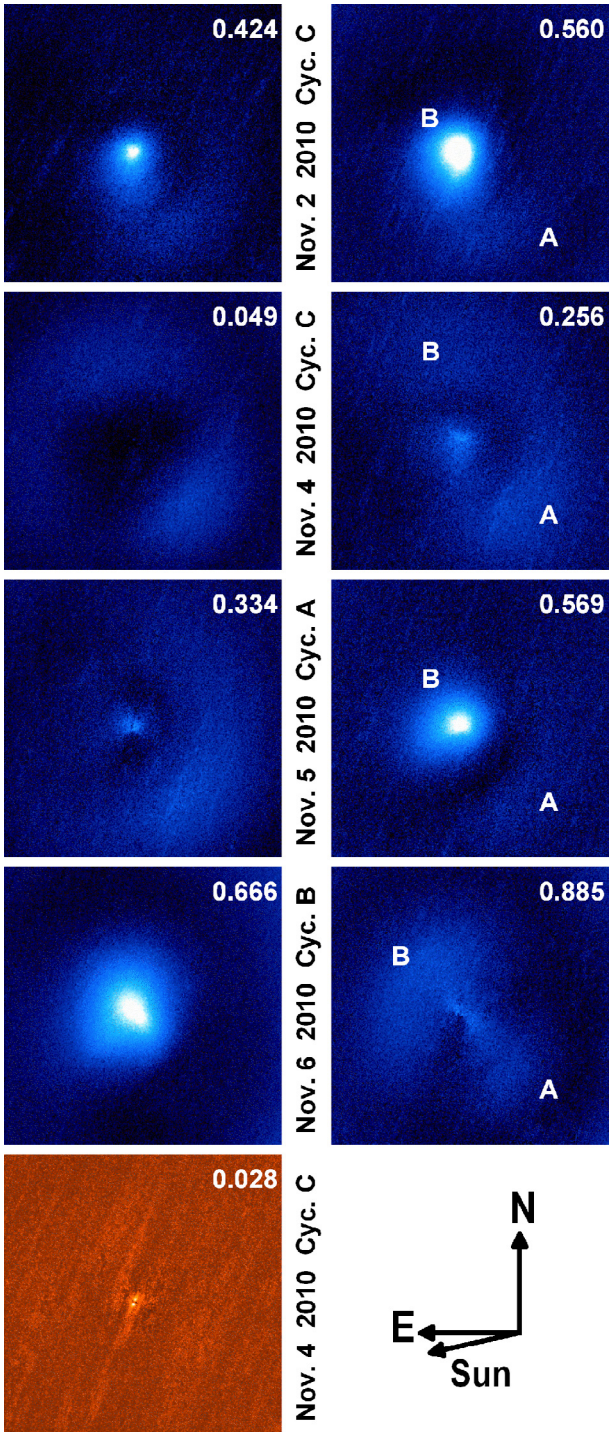

Fig. 1. First and last residual images of CN for each night. The *bottom left panel* shows the typical residual image of the dust coma. Dates and cycles (see text for details) are displayed. Phases with respect to the 18.32 h cycle are shown in the *upper-right* corners. The field of view is 6.4 arcmin or 43.8×10^3 km at the nucleus.

cometary dust from the signal in the molecular filters, it is obvious that our CN and C_3 images still contain a dust contribution. This contribution is very weak, though, as 103P has a very low dust-to-gas ratio (Schleicher 2010). Furthermore, the dust images processed with our *iterative image decomposition*, show no transient structures (see Fig. 1). This means that the light contribution produced by dust is totally contained in the stationary CN and C_3 profiles, hence the *residual images* contain pure information about the variability of the molecular coma.

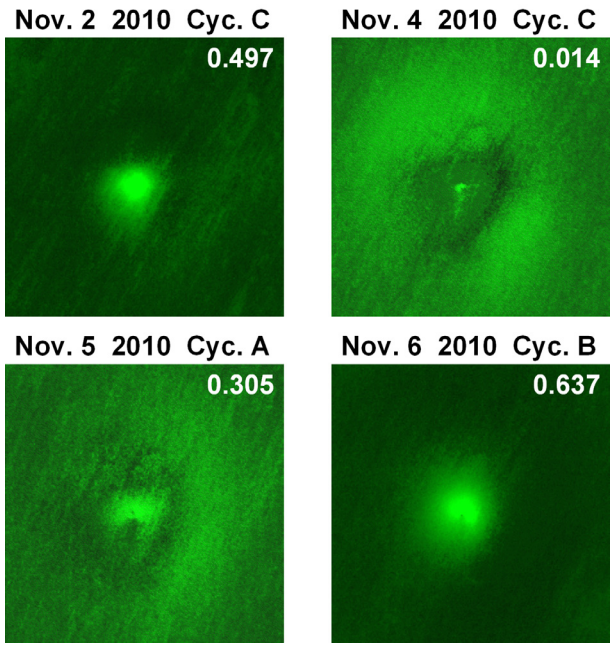

Fig. 2. Images of C_3 obtained by stacking the nightly series of the residual frames to increase the signal-to-noise ratio. Dates and cycles (see text for details) are displayed above the frames. Phases with respect to the 18.32 h period are shown in the *upper-right* corners. Orientation and image scale are the same as in Fig. 1.

3. CN and C_3 transient structures

Our *residual images* for CN and C_3 show the evolution of the transient structures over the four 4 nights of November 2, 5, and 6, 2010. Part of the whole set of data for CN is presented in Fig. 1 (the complete, chronologically ordered series can be seen as a video clip in Animation1). To show how the CN coma evolved with time, in Fig. 1 we present the first (left column) and last (right column) *residual image* for each night. In Fig. 2, we show nightly averaged snapshots for C_3.

Figures 1 and 2 reveal transient features of different kinds, and show that the CN and C_3 structures are strongly correlated. This means that both molecular environments behaved in very similar ways. To analyse the coma evolution with time, we introduced the nomenclature used earlier by Drahus et al. (2011). Each *residual frame* corresponds to a given precession phase (changing from 0 to 1) and precession cycle (denoted as *A*, *B*, and *C*) of the threefold precession period (the *three-cycle* period). The phases are obtained using the precession period of 18.32 h (justified further in Sect. 5). The moment of the EPOXI encounter occurred at the precession phase of 0.5 at the middle of *cycle B*.

As can be seen in Fig. 1, our data cover almost the full precession cycle. During the four nights, we observed *cycles C*, *C*, *A*, and *B*, respectively. Although we covered all the three cycles, we never observed the same cycle and phase twice. In general, we can discern markedly enhanced CN production at phases close to 0.5 on November 2, 5, and 6, when the central shells appeared and brightened on November 2 and 5, and diminished on November 6. These shells expanded outward, bearing arc- and spiral-like structures, which are visible up to the early phases of subsequent cycles. The shape and temporal evolution of the structure from November 6 resembles a traditional corkscrew (cf. Fig. 1 and Animation1): the north-east part can be identified as a relatively massive handgrip and the narrower south-west pattern can be attributed to the spiral (although its

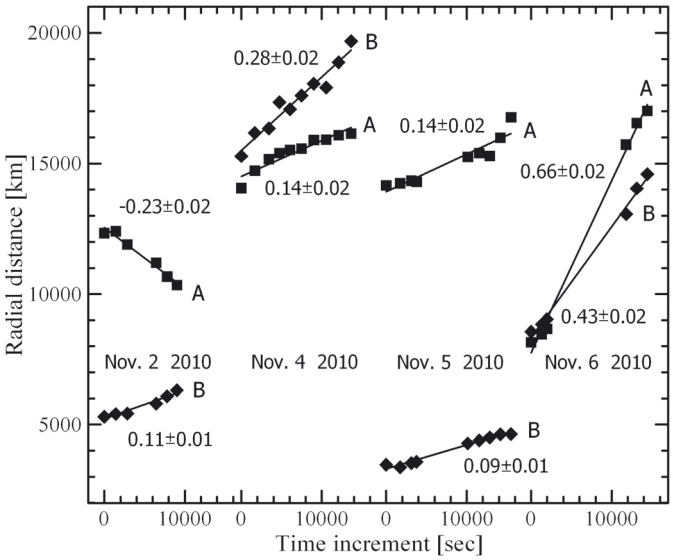

Fig. 3. Relation between the radial distances of the CN structure and time. The error bars are of the order of the symbol size and have been omitted. Linear fits and the expansion velocities in km s^{-1} are displayed.

spiral nature is not visible due to projection onto the sky). Similar corkscrew patterns had been previously reported for 103P (Knight & Schleicher 2011; Samarasinha et al. 2011).

Even a simple analysis reveals that all the three central shells have different profiles and behave differently in time. This can be seen in video clip Animation2, where we have applied a technique similar to *ring-masking* (A'Hearn et al. 1986) to the *residual images*, to enhance the contrast in the central region (from the individual pixel values, our method subtracts the smoothed radial profile of the azimuthal minimum). The features in the outer coma weakly correlate with their progenitors visible during the earlier cycles, which can be caused by the postulated excitation of the rotation state.

4. Kinematics of the CN features

To shed more light on the nature of the transient structures, we investigated their kinematics. The expansion velocity of the shells and arcs was measured separately in the south-west (A) and north-east (B) quadrants, as labelled in Fig. 1. We proceeded in a similar way as in our earlier work on 8P/Tuttle (Waniak et al. 2009). We first transformed the CN *residual images* to the rectangular frames arranging the radial distance from the nucleus in columns and the azimuth angle in rows. For every pair of these transormed images from a given night, we then determined the radial shift of the transient feature between both images. We cross-correlated the two frames, using a range of different displacements in the radial distance, to find the maximum of the correlation coefficient. Our approach ensures that sub-pixel precision is achieved in the shift determination even for diffuse features, but it does not determine the radial distance itself. Using the radial increments for all the pairs of *residual images* from each night and the radial distance of the chronologically first position derived from a crude estimation, we computed (using the LSQ approach) the radial distances of the successive positions of a given CN structure. The retrieved positions are presented in Fig. 3 together with the expansion velocities projected onto the sky plane, which were obtained from a linear fit.

In general, the projected velocities of different features are much smaller than the expansion velocity of 1.0 km s^{-1}, which is often assumed to be the canonical value for the gas coma at 1 AU (e.g. Combi et al. 2004). For November 2, 4, and 5, they range between 0.1 and 0.3 km s^{-1}, except for arc A on November 2, which exhibited movement toward the coma centre with the velocity of 0.23 km s^{-1}. This unusual arc does not correlate with any other arc- or spiral-like feature visible in Fig. 1. As the nature of this phenomenon remains unlear, we postpone its treatment to a future model analysis.

As shown by Waniak et al. (2009), CN produced by the photodissociation of HCN is a good tracer of its parent for the radial distances up to about one photochemical scalelength of HCN. Since the maximum radial distance considered in our analysis ($\sim 2 \times 10^4$ km) is only twice the scalelength for the cometary HCN ($\sim 10^4$ km), this condition is reasonably satisfied. Hence, the CN expansion velocity has to correlate well with the HCN expansion velocity. It is obviously hard to imagine that the expansion of the gas coma in 103P was indeed as slow as the projected expansion of the CN structures. The projection effect would be negligible only if either we observed the expansion of a spherical shell or the structures were aligned precisely on the sky-plane. The real expansion velocity was most probably significantly reduced by the on-sky projection, wich migth have in turn led to an inference of mass loss into a cone with a given opening angle and orientation. The November 6 data revealed a much higher expansion velocity of 0.66 km s^{-1} for arc A and 0.43 km s^{-1} for arc B, which can be possibly explained by a significantly altered geometry of the gas ejection, resulting in a strong reduction in the projection effect.

5. Periodicity in the CN data

The CN *residual images* were used as an input time series to search for periodicity. We separately investigated the (i) variability in the photometric signal, and (ii) repeatability of the transient features.

We performed aperture photometry of the central region of the CN coma, using a diaphragm with an optimum, 12-arcsec diameter (increasing the diaphragm size have resulted in a higher level of undesirable smoothness and phase delay of the near nucleus signal variability, but decreasing the diameter have increased the noise in the photometric data and the influence of imperfect on-comet tracking, variable seeing, and defocus). We verified that a diaphragm twice as small does indeed change the behaviour of the photometric data negligibly. That is because the expected aperture effect is stifled by the phase delay introduced by the photodissociation of the CN parent. The timescale for the aperture effect (i.e., the travel time between the aperture centre and its edge) is of the order of 10^3 s and the typical photodissociation timescale for the CN parent at 1 AU heliocentric distance is of the order of 10^4 s.

The periodicity was investigated using the weighted version of the phase dispersion minimization (PDM), developed by Drahus & Waniak (2006) from the classical non-weighted PDM (Stellingwerf 1978). The quality of the data phasing is probed by a parameter θ, which is the ratio of the variances of the phased to unphased data. The resulting PDM periodogram is presented in Fig. 4. The global minimum of θ occurs at the periodicity of 18.32 ± 0.30 h. Other minima are produced by the interference with a one-day cycle or represent harmonics of the basic frequency. Our result is an instantaneus synodic rotation period for the epoch UT 2010 Nov. 5.0835, i.e. for the middle moment of our run. Compared to other results obtained for similar dates, our solution is the same as the 18.32 ± 0.03 h periodicity detected in the HCN data (Drahus et al. 2011), agrees within the

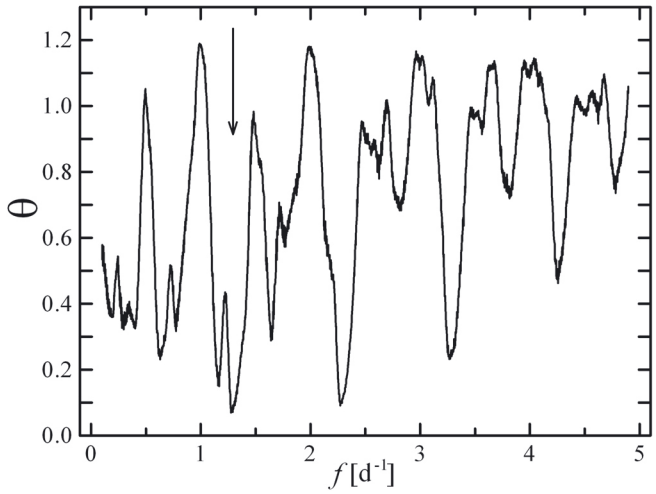

Fig. 4. PDM periodogram for our photometric data calculated using six bins and six covers. The optimal solution is found at the frequency of 1.310 d^{-1} (period of 18.32 h) and is indicated by an arrow.

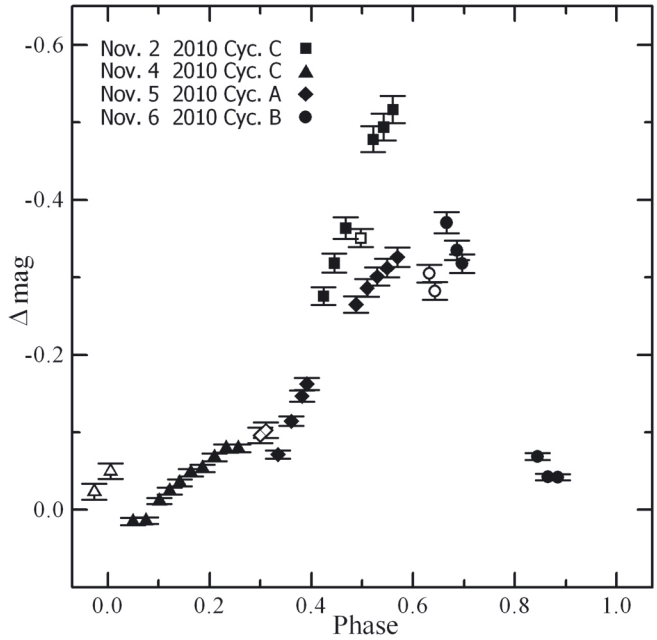

Fig. 5. Molecular light curves for CN (filled symbols) and C_3 (open symbols) phased according to the 18.32 h period. The moment of the EPOXI encounter has a phase 0.5 of *Cycle B*.

errors with the periods of 18.34 ± 0.04 h from the EPOXI photometry (A'Hearn et al. 2011) and 18.195 ± 0.010 h obtained from radar Doppler imaging (Harmon et al. 2011a), and is similar to the periods of 18.7 ± 0.3 h (Knight & Schleicher 2011) and ~18.8 h (Samarasinha et al. 2011) inferred from the repeatability of the CN coma profile.

The light curve phased according to the period of 18.32 h is displayed in Fig. 5, where we present the magnitude differences between the *residual frames* and the time-invariant average coma profile produced by the *iterative image decomposition*. Since the latter can be contaminated by dust (in contrast to the *residual images*; cf. Sect. 2), the presented light curve can be slightly deformed. For comparison, the C_3 photometric data are also presented in this plot. Although the C_3 signal might be contaminated by dust more strongly than CN, the photometric variability is comparable for both radicals. The maxima of the

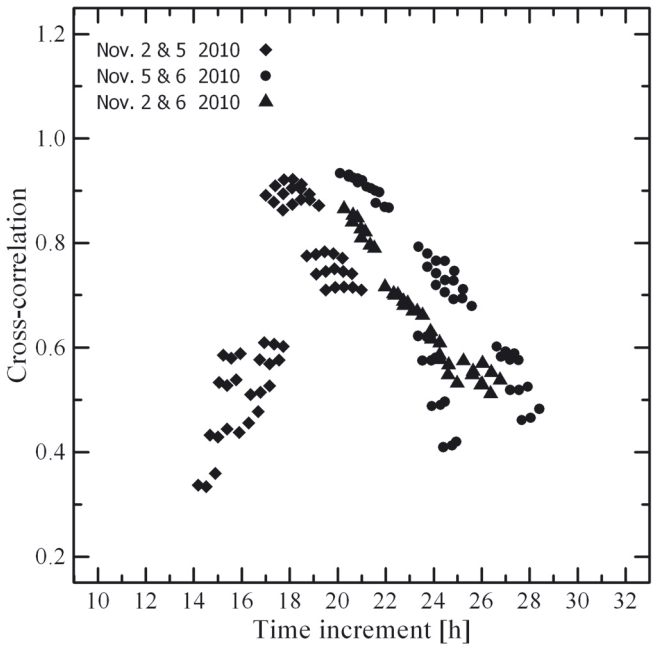

Fig. 6. Cross-correlation of the central CN shells between three nights. Multiples of the 18.32 h period have been subtracted from the actual time increments to obtain differences closest to the single period.

CN signal visible close to phase 0.5 may be related to the periodical insolation of the smaller tip of the elongated nucleus, which was active during the EPOXI encounter. Figure 5 shows that the maximum levels of the CN signal most probably differ noticeably for *cycles A*, *B*, and *C*. The secondary increase in the CN signal at phases ~0.25 of *cycle C* (November 4) is related to the weak central enhancement (see Fig. 1) and can be attributed to less active vents.

Another approach to investigating the periodicity in our *residual images* of CN is to analyse the repeatability of the CN transient structures based on the cross-correlation of the patterns in the *residual frames*, which is independent of the signal and measures the real similarity of the profiles. Although this procedure uses a different parameter than we used in our previous studies of comet 8P/Tuttle, the philosophy behind it does not change, and is described in Waniak et al. (2009). Because the outer CN structures, detached from the central features, heve a diverse range of profiles and expansion velocities, we compared only the central features visible on November 2, 5, and 6. The resulting set of cross-correlation parameters related to the time increments between the two exposures is presented in Fig. 6. Unfortunately, none of the dependences characterising the three pairs of nights have a clear maximum that could be used to precisely measure the period. While the plot is not as convincing as the photometric result in Fig. 5, it nevertheless provides an independent confirmation of our solution. We note the relatively high levels of cross-correlation, which reach up to 0.95 for November 2 and 5, and November 5 and 6. Even though the central shells observed on November 2, 5, and 6 appear to differ at first sight (see Fig. 1), the quantitative analysis shows that in general their patterns are similar.

6. Differences between the nucleus precession cycles

We first compare the behaviour of the CN coma in three consecutive precession cycles: *cycle A*, *B*, and *C*, which we observed

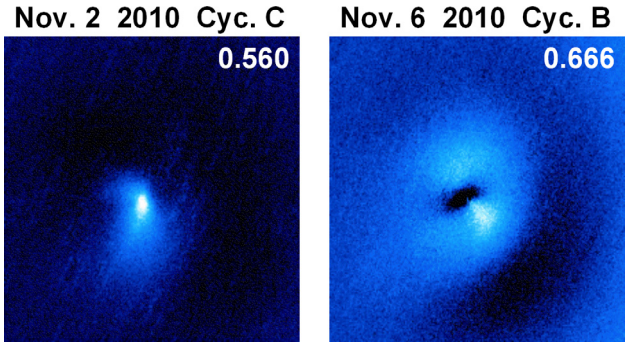

Fig. 7. Comparison of the transient structures in the CN coma on November 2 (*Cycle C*) and November 6 (*Cycle B*). *Each panel* presents the result of the subtraction of the *reference residual image* (November 5) from the actual *residual frame*. Phases are displayed in the *upper-right* corners. Orientation and image scale are identical as in Fig. 1.

during the production-rate maxima on November 2 (*cycle C*), 5 (*cycle A*), and 6 (*cycle B*). After analysing the behaviour of the central CN shells in the *residual images* (Fig. 1), and taking into account that we found (Fig. 6, Sect. 5) a stronger correlation level for the pairs of nights November 2 and 5, and November 5 and 6 than for November 2 and 6, we assumed that on November 5 (*cycle A*), we observed the most common and least structured pattern, which is related presumably to the most quiescent precession cycle. Taking this CN-shell profile from November 5 (*cycle A*) as a reference, we monitored how the central shells for November 2 (*cycle C*) and November 6 (*cycle B*) differ both from it and each other. We stacked the last four *residual images* from November 5 in order to increase the signal-to-noise ratio (S/N). We then subtracted this *reference pattern* from the *residual images* for November 2 and 6.

Figure 7 presents one example of the subtraction result for November 2 and one for November 6. The striking difference is easily visible. While on November 2 a bright jet directed southward was present, the November 6 image shows an elliptical envelope with a pair of bright spots. The brightness of the jet visible on the first night was increasing with time, and then it diminished a little. This caused the CN signal in our aperture to increase to its highest level observed during the whole run. On the night of November 6 (*cycle B*) the CN pattern closely resembled the CN structure from November 4 (*cycle C*) but was about two times smaller. The position angles of the bright spots from November 6 correlate very well with the position angles of similar features observed on November 4; they differ by 1° and 10° for structures A and B respectively, but this is of the order of the error bars. The reason for this similarity is that we observe different evolution stages (phase difference ~0.4) of the same structure, which appears periodically every three precession cycles. More precisely, these are the similarities between two different *cycles B*: one observed on November 6 and the other one preceding *cycle C* on November 4. We note, however, that both of these cycles exhibited different profiles of the CN features and dissimilar evolution. Moreover, the CN structures visible on November 4 moved slowly (0.14 km s^{-1} for part A and 0.28 km s^{-1} for feature B), whereas the structures for November 6 expanded much more rapidly (0.66 km s^{-1} and 0.43 km s^{-1} for structures A and B, respectively). Taking into account the very stable radial evolution of the corkscrew structure on November 6 (especially its south-west part), which did not exhibit either a spiral or wavy pattern, we suspect that this phenomenon was created by a fan with a relatively large opening angle enclosing the Earthward direction. The fan was rotating as the nucleus was rotating about the precession axis, which was also enclosed in this fan. The reason for this flat feature having such a large extent could be an appropriately oriented deep trench. Such a topographic element could lie along the border between the "waist" region and one of the nuclear lobes.

To explain the unexpected rise in the expansion velocity for this corkscrew pattern compared to the slowly moving CN features on the previous nights, the projection effect must have a significantly different influence. If our interpretation of the corkscrew structure was true, the on-sky projection would not have markedly affected the observed velocity on November 6 and hence it should be close to the real expansion velocity of the gas. This possibility implies that the opening angle of the fan producing the corkscrew structure was indeed huge compared to the opening angle of the CN ejection on November 4.

Comet 103P presents the clear dissimilarities in the CN transient patterns and their on-sky kinematics (see Sect. 4) for successive *cycles A*, *B*, and *C*. Similar variations in the line-of-sight kinematics of HCN, which is the most likely progenitor of CN, were reported by Drahus et al. (2012). The most natural explanation seems to be one of a typical gas flow velocity of the order of 1 km s^{-1} and a variation in the direction of the dominant gas ejection, which changes markedly from one cycle to another. The precession-roll scenario, proposed by A'Hearn et al. (2011), appears to provide a plausible explanation; it also closely relates to the extraordinary spin-down of the comet's nucleus caused most probably by the jet effect, which may also be responsible for the excited mode of rotation (e.g. Gutiérrez et al. 2003). In this case, one and the same active vent (e.g. the region recorded by EPOXI on the smaller tip of the nucleus) can eject matter in different directions and other vents can also be insolated during some or all of the precession cycles.

Since the three consecutive precession cycles produced different coma structures, it is interesting to examine whether these structures also evolved differently. Analysing video clip Animation2, we conclude that the expansion of the central shell observed on November 2 (*cycle C*) varied substantially from the behaviours observed on November 5 (*cycle A*) and 6 (*cycle B*). The former case represents an expanding, spiral-like structure in the northern part of the central feature. To ensure that this is not an artefact produced by our version of the *ring-masking* procedure (used to generate video clip Animation2), we verified the result using simple algebra for the *residual images*. To enhance the S/N, we stacked image #1 with #2, and #4 with #5 from November 2, and also #4 with #5, and #8 with #9 from November 5. Consequently, for each night we obtained a pair of images with time differences of 2.1 and 2.2 h for November 2 and November 5, respectively. We then subtracted the earlier image from the later one in each pair (all the frames having already been carefully normalized before). These differential images (Fig. 8) clearly illustrate the evolution of the central CN patterns as the difference of signals correlates with the time increment, i.e. higher values mean later stages of evolution. The results confirm our previous findings. On November 2, we observed the rotating spiral-like structure produced by a clockwise nucleus precession projected on the sky. This case resembles the well-developed spirals reported for 103P in September-October (see e.g. Samarasinha et al. 2011). The ellipsoidal shell observed on November 5 expanded highly symmetrically. This behavior is fully consistent with the scenario of gas ejection into a wide cone enclosing the Earthward direction. The prolateness of this envelope is controlled by the nucleus precession, which changes the orientation of the active tip during the insolation

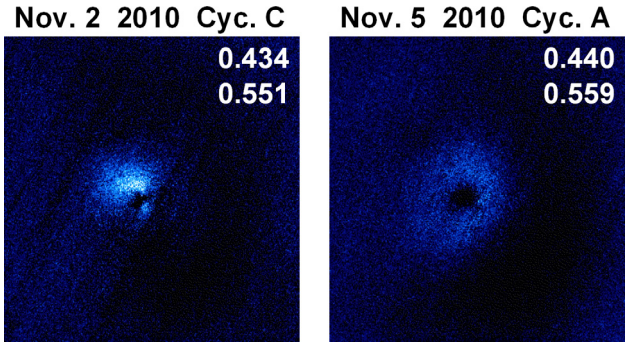

Fig. 8. Evolution of the central CN shell observed on November 2 (*Cycle C*) and November 5 (*Cycle A*). The behaviour in time is displayed by the result of the subtraction of the earlier exposure from the later one. Precession phases are shown in the *upper right* corners. Orientation and image scale are the same as in Fig. 1.

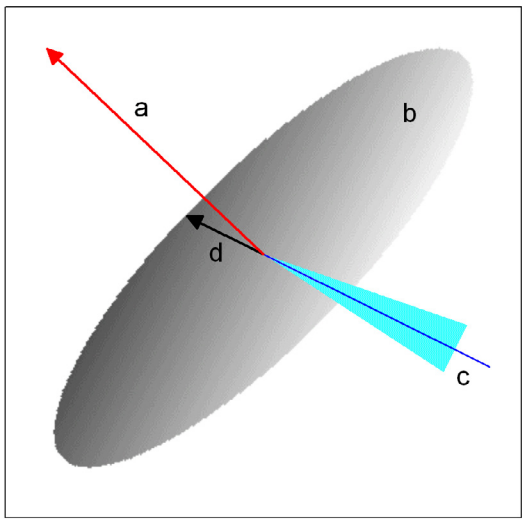

Fig. 9. Sketch illustrating how the orientation of the rotation axis was determined. This is an on-sky projection with a similar orientation to Fig. 1. Circular plane ***b*** is perpendicular to vector ***a***, which represents the direction of the shortest axis of inertia of the comet's nucleus. Line segment ***c*** shows the on-sky direction of the axis of the corkscrew pattern. Angular momentum vector ***d*** indicates our solution, which should be located at plane ***b***, and its on-sky projection should coincide with line segment ***c***.

phase producing the typical spiral that is visible almost completely edge-on on this date. A similar situation occurred on November 6.

The dissimilarity in the evolution of the central CN shell noticed between *cycles C* and *A* may be caused by a roll about the longest axis of the nucleus (A'Hearn et al. 2011). It is sufficient that the active vent, which occupies the smaller tip of the nucleus, is shifted off the roll axis.

7. Orientation of the nucleus rotation axis

We determine the orientation of the rotation axis assuming for simplicity that the nucleus was a SAM rotator whose spin axis is close to the precession axis. We have noted in Sect. 6 that the corkscrew structure (especially its south-west part) that was visible on November 6 expanded strictly radially and that the position angles of its expansion direction correlate with the traces of the corkscrew pattern seen on November 4. Hence, for different precession cycles there is one distinct direction, which we attribute to the on-sky projection of the rotation axis of 103P. If this was true, the south-west section of the corkscrew structure would have been created by a circumpolar gas jet. As the on-sky velocity of this pattern was relatively high, it expanded in a direction far from the line of sight, forming a conical structure that is consistent with our observations. Thus, we assumed that the symmetry axis of the south-west part of the corkscrew structure corresponds to the on-sky projection of the nucleus rotation axis.

In a subsequent step, we used the *in situ* determination of an instantaneous orientation of the longest axis of 103P's nucleus during the EPOXI flyby (A'Hearn et al. 2011), which we assumed represents the shortest axis of inertia. It is obvious that the rotation axis must lie in the plane perpendicular to this axis, as shown in Fig. 9. On the other hand, the on-sky projection of the rotation axis should coincide with the direction of the south-west part of the corkscrew pattern. After combining both restrictions, we found that the orientation of the north rotation pole (sense of spinning is determined in Sect. 6) was RA = 122° and Dec = +16° (epoch J2000.0). The error in our determination is dominated by the validity level of our assumptions, which is very difficult to estimate. If our assumptions were strictly satisfied, the obtained circular error would be 2°, which we computed by propagating the uncertainty in both the position angle of the south-west part of the corkscrew structure and the orientation of the longest nucleus axis (A'Hearn et al. 2011).

A'Hearn et al. (2011) found that the direction of the total angular momentum (close to the precession axis) is equal to RA = 17 ± 11° and Dec = +47 ± 2°. Radar Doppler imaging (Harmon et al. 2011b) gave the result RA = 332° and Dec = +20°. The analysis of the CN coma structures performed by Knight & Schleicher (2011) shows the axis direction of RA = 257° and Dec = +67° with an uncertainty of 15°, and Samarasinha et al. (2011) obtained RA = 345°, Dec = −15° with an uncertainty of 20°. Although, it is hard to obtain a coherent picture from these results, all the solutions (including ours) are preliminary at this stage.

8. Comparison of CN and HCN

Since we have found a remerkable coincidence between the rotation periods derived from the HCN and CN data (cf. Sect. 5), we also examined the correlation between both molecules, by comparing the variability in the relative photometry of CN (Sect. 5) with a series of the HCN main-beam brightness temperatures from IRAM 30-m (the latter being part of the observing material obtained by Drahus et al. 2011, 2012). Both the CN photometry and the HCN data selected for comparison were collected around the same time and in part simultaneously. Figure 10 presents this comparison, where the data are phased in the same way as before (cf. Sects. 3 and 5), and identically for all practical purposes with Drahus et al. (2011).

We should bear in mind that HCN was monitored with a beam size three times smaller than the aperture used for our CN photometry. Hence, the CN variability might have been phase-delayed from that of HCN. Such an aperture effect was discussed in Sect. 5 and found to be negligible. The markedly smaller amplitude of the variability of CN may result from the smoothing introduced by the finite lifetime of the CN parent ($\sim 10^4$ s for HCN). In general, both light curves correlate quite well in the active phases and far more poorly during the quiescent periods. Perhaps CN in 103P originates from two different sources, each behaving differently. One source could be related to insolated active vents and the other one to either different parts of the nucleus surface or a volume source surrounding the nucleus, such as e.g. the "snowflakes" detected by EPOXI

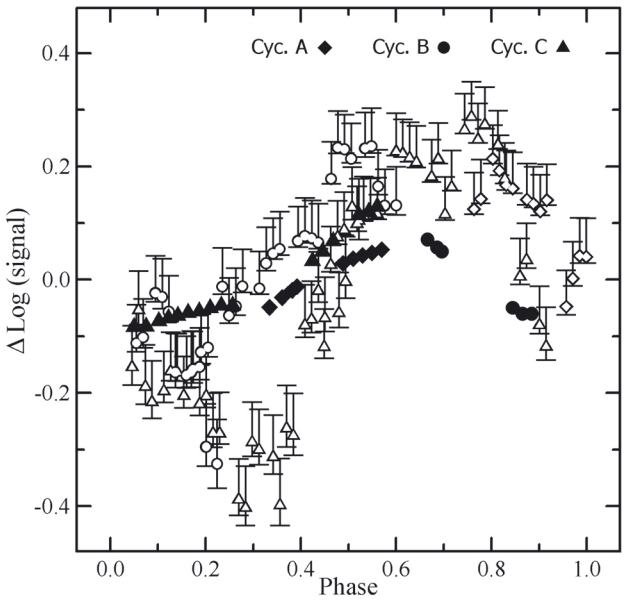

Fig. 10. Comparison between the molecular light curves of CN (see text) and HCN (from Drahus et al. 2011). The HCN signal is represented by the line area measured in the beam of 8.8-arcsec FWHM. The light curves are calculated with respect to the mean levels, and phased according to the 18.32 h period. The filled symbols are used for CN and the open symbols for HCN, while the symbol shape indicates the *three-cycle* component. The error bars for CN are of the order of the symbol size and have been omitted.

(A'Hearn et al. 2011). To examine the correlation between HCN and CN more deeply, a non-steady-state model of the HCN-CN coma has to be build, which is the subject of one of our ongoing studies.

9. Conclusions

We present the main conclusions of our study below:

1. Our image processing of our CN and C_3 observations has revealed transient structures in the gas coma of 103P. Both radicals formed very similar features at moments close in time. Our CN and C_3 photometry are found to be consistet with each other. We conclude that the progenitors of CN and C_3 were emitted from the same regions of the nucleus, which implies its homegeneity with respect to origin of both the CN and C_3 parents.
2. The CN signal varied with a period of 18.32 ± 0.30 h at the epoch of our observations (UT 2010 Nov. 5.0835), which is identical to the period measured for HCN around the same time. The variability of HCN correlates with the behaviour of CN, suggesting that HCN was a major donor of CN.
3. The CN structures expanded with projected velocities of between 0.1 km s^{-1} and 0.3 km s^{-1}, except for November 6, when the velocity increased by up to 0.66 km s^{-1} in the south-west part of the corkscrew pattern.
4. The CN shells appearing in the central part of the coma at the phases of boosted CN production, have profiles, which in general correlate with each other. They were most probably generated by periodic insolation of the smaller tip of the nucleus, which was active during the EPOXI encounter. The CN profiles observed during the consecutive *cycles A*, *B*, and *C* differed in details. A modest CN boosting was observed in *cycle A* (November 5), a corkscrew pattern was present during *cycle B* (November 6), and a southern jet was visible in *cycle C* (November 2). They may suggest that for different cycles different nucleus parts, carrying different vents, were exposed to the solar radiation and active.
5. Although the corkscrew structure seems to have appeared every three precession cycles, the situation did not strictly repeat itself (with different profiles and kinematics).
6. Combining the results of our image analysis with the instantaneous nucleus orientation from EPOXI and assuming a principal-axis rotation mode, we inferred that the orientation of the spin axis is equal to RA = 122° and Dec = +16° (epoch J2000.0).

Acknowledgements. The authors gratefully acknowledge observing grant support from the Institute of Astronomy and Rozhen National Astronomical Observatory, Bulgarian Academy of Sciences. W. Waniak acknowledges the financial support of the Nicolas Copernicus Foundation for Polish Astronomy. M. Drahus was supported by a NASA Planetary Astronomy grant to David Jewitt. The authors thank the referee, M. Belton, for very helpful suggestions.

References

A'Hearn, M. F., Hoban, S., Birch, P. V., et al. 1986, Nature, 324, 649
A'Hearn, M. F., Belton, M. J. S., Delamere, W. A., et al. 2011, Science, 332, 1396
Arpigny, C., Weaver, H. A., A'Hearn, M. F., & Feldman, P. D. 1993, LPICo, 810, 17
Belton, M. J. S. 1991, in Comets in the Post Halley Era, ed. R. L. Newburn Jr., M. Newgebauer J. Rahe (Dordrecht: Kluwer Academic Press), 691
Belton, M. J., & Drahus, M. 2007, BAAS, 39, 498
Belton, M. J. S., Mueller, B. E. A., Julian, W. H., & Anderson, A. J. 1991, Icarus, 93, 183
Belton, M. J. S., Fernandez, Y. R., Samarasinha, N. H., & Meech, K. J. 2005, Icarus, 175, 181
Belton, M. J. S., Meech, K. J., Chesley, S., et al. 2011, Icarus, 213, 345
Bockelée-Morvan, D., & Crovisier, J. 1985, A&A, 151, 90
Combi, M. R., Harris, W. M., & Smyth, W. H. 2004, in Comets II, ed. M. C. Festou, H. U. Keller, & H. A. Weaver (Tuscon: University of Arizona Press), 523
Colangeli, L., Epifani, E., Brucato, J. R., et al. 1999, A&A, 343, L87
Crovisier, J., Encrenaz, T., Lellouch, E., et al. 1999, ESA SP, 427, 161
Davidsson, B. J. R. 2001, Icarus, 149, 375
Drahus, M., & Waniak, W. 2006, Icarus, 185, 544
Drahus, M., Jewitt, D., Guilbert-Lepoutre, A., et al. 2011, ApJ, 734, L4
Drahus, M., Jewitt, D., Guilbert-Lepoutre, A., Waniak, W., & Sievers, A. 2012, ApJ, in press [arXiv:1202.3194]
Epifani, E., Colangeli, L., Fulle, M., et al. 2001, Icarus, 149, 339
Farnham, T. L., Schleicher, D. G., & A'Hearn, M. F. 2000, Icarus, 147, 180
Fray, N., Bénilan, Y., Cottin, H., Gazeau, M. C., & Crovisier. J. 2005, Planet. Space Sci., 53, 1243
Gutiérrez, P. J., Jorda, L., Ortiz, J. L., & Rodrigo, R. 2003, A&A, 406, 1123
Harmon, J. K., Nolan, M. C., Howell, E. S., Giorgini, J. D., & Taylor, P. A. 2011a, ApJ, 734, L2
Harmon, J. K., Nolan, M. C., Howell, E. S., Giorgini, J. D., & Taylor, P. A. 2011b, 42nd Lunar and Planetary Science Conf., 1480
Jewitt, D. 1992, in Proc. 30-th Liège Int. Astrophys. Colloq., ed. A. Brahic, et al. (Liège: University of Liège), 85
Jockers, K., Credner, T., Bonev, T., et al., 2000, Kinematika i Fizyka Niebesnykh Tel Suppl., 3, 13
Knight, M. M., & Schleicher, D. G. 2011, AJ, 141, 183
Meech, K. J., Belton, M. J. S., Mueller, B. E. A., Dicksion, M. W., & Li, H. R. 1993, AJ, 106, 1222
Meech, K. J., A'Hearn, M. F., Adams, J. A., et al. 2011, ApJ, 734, L1
Samarasinha, N. H., Mueller, B. E. A., Belton, M. J. S., & Jorda, L. 2004, in Comets II, ed. M. C. Festou, H. U. Keller, & H. A. Weaver (Tuscon: University of Arizona Press), 281
Samarasinha, N. H., Mueller, B. E. A., A'Hearn, M. F., Farnham, T. L., & Gersch, A. 2011, ApJ, 734, L3
Schleicher, D. 2010, IAU Circ., 9163
Stellingwerf, R. F. 1978, ApJ, 224, 953
Waniak, W., Borisov, G., Drahus, M., et al. 2009, EM&P, 105, 327
Weaver, H. A., Feldman, P. D., McPhate, J. B., et al. 1994, ApJ, 422, 374

Appendix A: Image cleaning procedure

With the aim of removing cosmic ray hits (CRH) and stellar profiles elongated by non-sidereal tracking, we grouped consecutive images into pairs and compared the first frame with the second frame in each pair. We took advantage of the statistical independence of the CRHs in different frames, and that in two consecutive frames a given stellar trail occupies separable regions (the 40-s CCD readout time corresponds to three arcsec of cometary motion). We subtracted and averaged images in pairs, obtaining two series of images: one with differential frames and an other with mean frames. For each differential image, we correlated its noise statistics with the mean signal in the corresponding average frame. Using the relation between the noise level and mean signal, it is possible, for a given pixel, to estimate the dispersion in the signal in the differential frame. When the pixel value in the differential image was higher than $K\sigma$ (i.e. a factor of K above the local noise), we flagged it in an auxiliary binary mask frame. As the stellar patterns in the auxiliary mask frames contain regions with disconnected pixels (external envelopes of bright stars and whole patterns for stars at the noise limit), we produced compact patterns improving pixel connectivity. We used the closing-like procedure based on the local surface density of the flagged pixels. For a given pixel, the density was probed in a small circle surrounding this pixel and compared with the limiting value. This value was determined using the trial-and-error procedure. Above this limit, the pixel was kept flagged and vice versa. This stage of image processing was completed by synthesizing clean stacks. In the regions where neither CRHs nor stellar trails were detected, the mean values of both frames were taken. Otherwise, the values from the image with no detection were accepted. As the comet was observed in relatively dense stellar fields, the profiles of different stars occasionally overlapped in the images from one pair. In these situations, the stellar trails were masked and filled using interpolation. By stacking two consecutive images, we increased the S/N except for the regions occupied by the stellar profiles or CRHs. We note that in rare cases one and the same frame was used to create two consecutive pairs. Obviously, such pairs are not independent, but let us use the entire nightly material, even if the number of single images is odd. Figure A.1 presents one example of how our cleaning procedure is able to remove unwanted objects from the comet image.

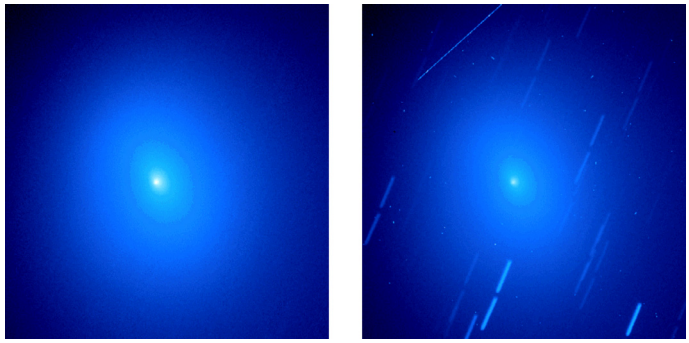

Fig. A.1. Result of removal of CRHs and stellar profiles by the cleaning procedure (*left panel*). For comparison, the *right panel* shows the result of simple stacking of the same two frames. Date of observation is UT 2010 Nov. 7.1375. The field of view is 6.4 arcmin. North is up and east is to the left.